Proceedings of the 9th World Congress on Momentum, Heat and Mass Transfer (MHMT 2024)
London, United Kingdom – April 11 – 13, 2024
Paper No. CSP 110
DOI: 10.11159/csp24.110

Determination of Kinetic Parameters of Rapid Pyrolysis of Ammonium Perchlorate

Prathamesh Phadke[a], Shani Saha[a*], Jay Patel[a], Rohit Sehrawat[b], Arvind Kumar[b], Arindrajit Chowdhury[a], Neeraj Kumbhakarna[a,]
[a]Department of Mechanical Engineering, Indian Institute of Technology Bombay, Mumbai-400076, India
[b]High Energy Material Research Lab, Pune-411021, India
*Corresponding author- shanisaha10@gmail.com

Abstract - A laser pyrolyser setup is developed to achieve isothermal conditions using a heating rate of up to ~10^5 °C.s^{-1} for rapid pyrolysis of a sample. It provides mechanistic information about the decomposition behavior of the sample during combustion, typically in the condensed phase. Data about the kinetics of chemical reactions occurring in the condensed phase during combustion is not derived from ab initio techniques, but rather by fitting the variation of linear burning rate with pressure with appropriate kinetic parameters. This leads to a wide variation of chemical kinetic parameters governing the decomposition of the same solid propellant ingredient, such as the commonly used oxidizer, ammonium perchlorate (AP). Therefore, the laser pyrolyser/Fourier transform infrared (FTIR) spectroscopy was used to study the rapid pyrolysis of AP at 1 bar. The concentration profiles of the evolved gases were used to develop the global reaction mechanism. The global reaction mechanism was found as follows: $NH_4ClO_4 \rightarrow 1.09\ H_2O + 0.06\ HNO_3 + 0.56\ NO_2 + 0.18\ N_2O + 0.5\ Cl_2 + 0.71\ O_2 + 0.88\ H_2$ with kinetic parameters as pre-exponential factor (A) = 6.6x10^7 s^{-1}, activation energy (E_a) = 108 kJ.mol^{-1}. Kinetic parameters of the same AP from thermogravimetric analysis are A = 5.6 x 10^5 s^{-1}, and E_a = 100 kJ.mol^{-1}. This suggests that kinetic parameters obtained from slow heating experiments predict a reaction rate significantly lower than that observed under high heating rates. Therefore, the raw data generated from rapid pyrolysis would be useful to develop detailed chemical reaction mechanisms for the chosen ingredients which would further improve the fidelity of the solid propellant combustion models.

Keywords**:** Ammonium perchlorate; Laser pyrolyser; Condense phase; Activation energy; Pre-exponential factor

1. Introduction

In the realm of solid propellant combustion, the chemistry governing the condensed phase remains elusive. To precisely model the combustion of solid propellants, understanding the reactions in the condensed phase and obtaining their kinetic parameters are imperative. The literature review section elucidates the significance of and the existing gap in understanding the condensed phase.

Commonly employed commercial instruments for studying the decomposition of energetic materials, such as TGA and DSC, typically operate with a maximum heating rate of ~10 °C.s^{-1}. However, to authentically examine solid propellant samples, it is crucial to mimic the heating rates observed during combustion, which can reach ~10^5 °C.s^{-1}. Existing experimental setups, such as SMATCH/FTIR [1], T-Jump/FTIR [2], and CRT-MS/FTIR [3], offer high heating rates (2 x 10^4 °C.s^{-1}, 3.5 x 10^2 °C.s^{-1}, and 1.5 x 10^3 °C.s^{-1}, respectively) for studying condensed phase decomposition while enabling species measurement. Whereas, Our developed setup presents three notable advantages: first, capable of achieving isothermal conditions using higher heating rate of up to ~10^5 °C.s^{-1}, and can measure species during rapid pyrolysis of sample at isothermal conditions; second, ease of replacing the foil supporting the sample at no additional cost in case of damage, unlike the time and cost-intensive process of replacing the heating filament in electrical probes of T-Jump/FTIR [2] and third, can measure mass change at high heating rate and pressure. However, the third advantage of our work, i.e. integration of mass balance with the laser pyrolyser, is still in progress. Hence the results obtained after implementation of only the first two advantages from our experimental setup are reported in this work. Details of our setup are elaborated in the experimental section.

Ammonium perchlorate (AP), is widely used as an oxidizer in missiles and boosters for space launch vehicles. Thus, understanding the behavior of AP during combustion is key to designing the propellant formulations used in the solid rocket motors for specific mission requirements. However, current combustion models which are used to design the solid rocket motors lack the kinetic decomposition process information at high heating rates. Hence, the focal point of this current work

is to analyze AP's condensed phase decomposition within the combustion context. Identifying and quantifying decomposition products is pivotal in comprehending condensed phase decomposition. These data become instrumental in developing accurate models and mechanisms for understanding the sample's condensed phase decomposition during combustion.

2. Literature Review

The combustion wave structure of an energetic material [4] typically consists of a solid-phase zone, condense-phase zone and gas-phase zone. Comprehensive reviews of the solid propellant combustion modelling have been published in the literature [5-7]. Due to the very complex nature of the condensed phase zone, very little information is available about it [8]. Initially, when the details about the condensed phase zone were not available, it was modelled as an infinitely thin region that is a source of reactants for the flame zone. The rate of evolution of the reactants was given by a single Arrhenius-type law. The granular diffusion flame model [9] and the models by Beckstead, Derr, and Price (BDP) [10] are some of the notable models which simulate the condensed phase region as an infinitely thin region. However, work done by Merzhanov [11], Strunin and Manelis [12] and Li et al. [13] emphasize the importance of the major role of the condensed phase zone in the prediction of combustion characteristics. Many researchers now agree that 70-90% of the heat from the propellant is released in the condensed phase region, at least up to 10-20 atm pressure [8]. It can be observed from the literature [14-19] that wherever the condensed phase is modeled as a global one-step reaction at the surface, the burn rate is linked to the surface temperature using the Arrhenius equation. The general form of the Arrhenius-type pyrolysis law is as follows:

$$\dot{r}\left(T_s\right) = A_r \times \exp\left(\frac{-E_s}{R_u T_s}\right) \tag{1}$$

Where, $\dot{r}$ - burn rate (m.s^{-1}), A_r - Pre-exponential factor for burn rate (m.s^{-1}), E_s- Activation energy related to the burning surface (J.mol^{-1}), R_u- Universal gas constant = 8.314 J.mol^{-1}.K^{-1} and T_s- Temperature of the surface (K).

The pyrolysis law given by Equation (1) is implemented in various alternate forms by different researchers. However, there exists significant uncertainty regarding the values of the pre-exponential factor (A) and the activation energy (Es) for the condensed phase processes of AP. In most of the models, the activation energy is assumed to be in the range of 80-120 kJ.mol^{-1} based on the linear pyrolysis experiments done with AP by Anderson et al. [20], Coates [21] and Powling et al. [22]. The value of the pre-exponential factor is chosen as the best-fit value which gives the least error between the simulated and experimental burn rate. Ramakrishna et al. [17] assumed the activation energy of the surface pyrolysis reaction to be 50 kJ.mol^{-1} using the intrinsic flame stability criterion and calculated the value of the pre-exponential factor to match the burn rate at one particular pressure. Kumar et al. [18] and Nagendra et al. [19] follow similar methodologies as that of Ramakrishna et al. [17] by tweaking the values of the activation energy and pre-exponential factor based upon experimental burning rates measured by the authors. Ermolin et al. [23] developed a detailed gas phase reaction mechanism. However, no attempt was made to develop a similar detailed reaction mechanism for the condensed phase. Brill et al. [24] analyzed the condensed phase decomposition of AP by decoupling it from the gas phase processes using a Temperature–Jump (T-Jump) / Fourier Transform Infrared (FTIR) spectroscopy technique. Despite providing great insight into the chemical reaction pathways, no information about the kinetics of the decomposition process was provided by the authors.

Thus, from the overall review of the literature published regarding the modelling of combustion of AP and experimental work regarding the condensed phase decomposition of AP, it becomes evident that available experimental data regarding the kinetics of the condensed phase decomposition of AP is insufficient. The determination of the condensed phase chemical kinetic parameters is crucial in the development of rationally sound combustion models, minimizing the reliance on numerous “floating” parameters.

3. Experimental

3.1 Experimental setup

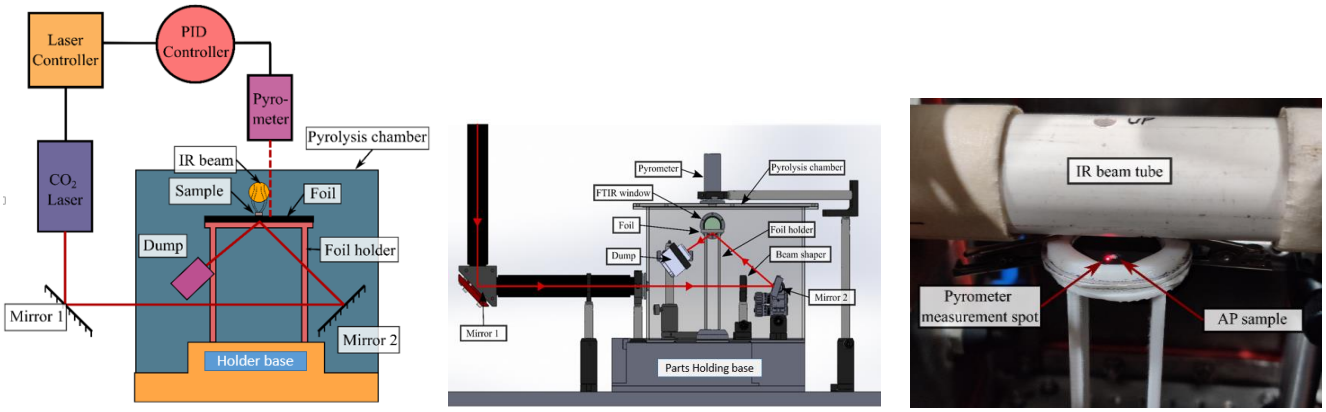

(a) (b) (c)

Fig.1. Schematic of working principle of laser pyrolyser. (b) 3D model of the CO2 laser beam delivery system with internal components of the pyrolysis chamber (c) Approx. 500 µg of AP was placed near the pyrometer measurement spot on the aluminium foil for the sample run.

Fig. 1(a) shows the schematic of the working principle of the laser pyrolyser. The sample is placed at the centre of an aluminium foil. The foil is held in position using a foil holder. This foil holder is screwed to the holder base. The sample, foil, foil holder, and holding base are enclosed inside a pyrolysis chamber to isolate them from the environment. The pyrolysis chamber has optical windows for the CO_2 laser beam as well as FTIR measurement. A non-contact IR pyrometer measures the temperature of the surface of the foil at some distance away from the sample. When switched on, the laser is directed toward the bottom of the foil by beam delivery optics (mirrors and windows). The laser is partly absorbed by the foil and partly reflected. The absorption of the laser by the foil increases the temperature of the foil and in turn, heats the sample placed on top of it. The reflected part of the laser is absorbed by the dump to avoid unwanted reflection and absorption inside the pyrolysis chamber. The pyrometer reads the surface temperature of the foil at some distance away from the sample. The temperature reading is passed to a PID controller which compares the reading with a pre-set final temperature. The PID controller supplies the control signal to the laser controller which in turn modulates the laser power as required to maintain the pre-set temperature.

Fig. 1(b) shows the 3D model of the pyrolysis chamber and the beam delivery system. Fig. 1(b) also shows the laser beam path inside the pyrolysis chamber which ultimately ends at the laser dump. The FTIR windows allow the IR beam from an FTIR spectrometer to pass just above the surface of the sample so that the decomposition products can be analysed. The pyrolysis chamber can be purged with any inert gas. All the components related to the beam delivery system and the pyrolysis chamber which are shown in Fig. 1(a) can be mapped to those in Fig. 2 except for the beam shaper. A beam shaper is an optical component that changes the energy distribution of the CO_2 laser beam and ensure uniform heating.

The FTIR spectrometer is coupled with the pyrolysis chamber using additional external adaptation supplied by Bruker. The FTIR beam is directed outside the instrument using external optical accessories so that the IR beam passes just above the foil inside the pyrolysis chamber. The IR beam is then focused on the external detector of the FTIR spectrometer which then passes the signal to the main unit for further processing. A tube bracket was added to the pyrolysis chamber to isolate the IR beam of the FTIR spectrometer from the CO_2 laser beam and its unwanted reflections. Fig. 1(b) shows the IR beam tube is placed in its position. The IR beam tube is made of PVC and two holes were drilled into it to allow the pyrometer beam to read the surface temperature as well as to allow the decomposition products to enter the IR beam region for

detection.For data acquisition, all measuring devices were connected to a PC. Bruker OPUS software is used to record and analyse the FTIR data. For temperature control settings, Sensor Tools software developed by Sensortherm is used.

3.2 Experimental procedure

Before experiments, the alignment of the CO_2 laser is checked. The list of things to do in an experiment run is as follows: 1) Place the foil holder with the foil on the holding base. 2) Ensure the pyrometer measurement spot is in the proper position. 3) Place the sample as shown in Fig. 1(c) Then place the IR tube in place. 4) Close the lid of the pyrolysis chamber. 5) Purge the chamber with nitrogen gas for 5 mins. 6) Turn the purge off. 7) Wait for 5 minutes for the movement of the gas inside the chamber to settle. 8) Trigger the background scan on the FTIR spectrometer (Let this time be t = -5 s). 9) 5 s after the completion of the background scan, trigger the sample scan on the FTIR spectrometer (t = 0 s). 10) Start the stopwatch (t = 0 s). 11) Fire the laser at t = 15 s.

Approximately 500 µg of the 50 µm AP sample is placed as close to the pyrometer measurement spot as possible. Fig. 1(c) shows the placement of the AP sample before the sample run. As the laser falls on the bottom of the aluminum foil, it heats the foil due to which the sample decomposes. The decomposition products of the sample (which evolve as gaseous products) enter the IR beam tube shown in Fig. 1(c). The gaseous products are detected by the FTIR spectrometer. Two FTIR spectrometer scans are performed in each experiment: the first is the background scan and the second is the sample scan. The sample scanning is done in rapid scan mode in which multiple scans are taken at fixed time intervals. For the current experiment, the spectrometer scans a total of 380 frames with a time interval of 0.086 s between each frame. Hence the total time for data acquisition is around 33 seconds.

For temperature measurement and control, a pyrometer and PID controller are used. The pyrometer measurement spot is located near the sample. The target for temperature measurement is the Pyromark-coated aluminium foil. The emissivity of the target is an input parameter required for the temperature measurement. For this particular case, an emissivity value of 0.9 was measured and validated against the data available in literature in which the same Pyromark paint was used to coat metal surfaces [25].

4. Results and Discussion

Fig. 2(a) shows that when the temperature program is executed, the temperature immediately starts rising and reaches the set temperature within a few milliseconds (~ 26 ms). The set temperature is held for 10 seconds as per the given input. Fig. 2(b) shows the zoomed-in view of the initial region highlighted in maroon colour in Fig. 2 (a). Around t = 0.055 s, the laser heating is initiated as seen from the jump in laser power from 0% to 95%. At t = 0.055 s, the foil is still at room temperature (~30 °C). To follow the input temperature program, the laser power is held constant at its maximum value of 95% from t = 0.055 s to t = 0.075 s during which the foil temperature rises from room temperature to ~440 °C. As the foil temperature approaches the set temperature, the laser power is reduced proportionally to the error between the actual temperature and the set temperature. The laser power drops to 0% once the measured temperature of the foil crosses the pre-set temperature at t = 0.081 s where the (at a measured temperature of 461 °C). Then the laser power again picks up and is modulated around 10-17% to hold the foil temperature constant at 450 °C. At t = 10 s, the temperature program is completed and the laser power is switched to 0%. Due to this, the foil temperature also drops back to room temperature.

The IR pyrometer used to measure and control the foil temperature has a lower limit of 180 °C. Hence, the recorded foil temperature in the time duration of t = 0.065 s to t = 0.081s was fit to a 3rd-degree polynomial to extrapolate the measurement back to room temperature and to calculate the heating rate. The extrapolated temperature profile is shown in Fig. 2(b). The heating rate of the foil and hence the sample can be calculated based on the extrapolated temperature profile values: at t = 0.055 s, T = 29.7 °C, and at t = 0.081 s, T = 461.2 °C. The heating rate is calculated in Equation (2)

$$\frac{dT}{dt} = \frac{T_2 - T_1}{t_2 - t_1} = \frac{(461.2 - 29.7)°C}{(0.081 - 0.055)s} = 16596 °C.s^{-1} \qquad (2)$$

Where, T – temperature in °C, t – time in seconds and subscripts 1 and 2 denote the two instances chosen for the calculation of the heating rate.

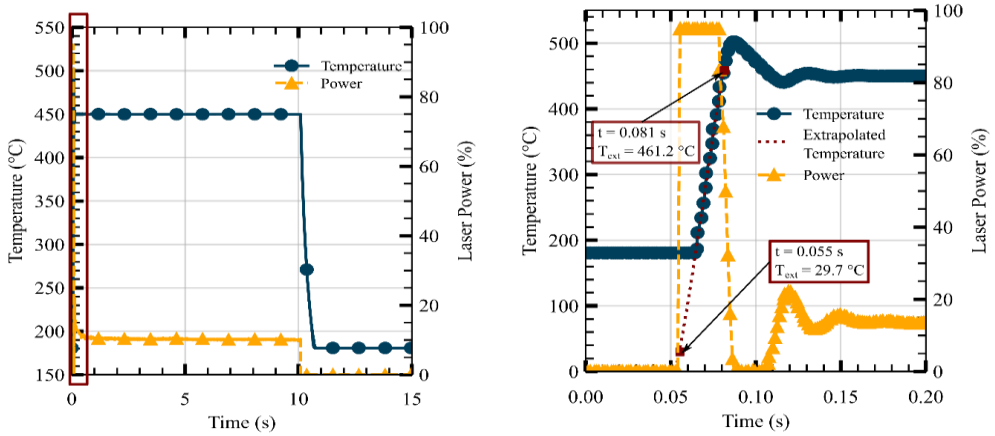

Fig. 2. The variation of temperature of the pyrometer spot with time as well as the laser power required to maintain the temperature. (a) Total time of the temperature program. (b) Zoomed-in view of the section highlighted in maroon in (a)

From Equation (2) it can be seen that the heating rate of the laser pyrolyser is of the same order as that of the T-Jump/FTIR setup and significantly greater than that of SMATCH/FTIR and CRT setups. Due to the inherent nature of a PID process, the temperature of the foil overshoots the set temperature by 50 °C reaching a value as high as 500 °C as can be seen from Figure 2(b). But the temperature quickly drops from the maximum value to the set value in a time duration of about 65 ms. Thus, the overshoot will not affect the physical and chemical nature of the sample significantly before it reaches the set temperature.

From the transmittance spectra, the major decomposition products of AP can be identified as H_2O, NO_2, N_2O, and HNO_3. Some small amounts of CO_2 and H_2O were already present during the start of the experiment as a residual of the incomplete purging of the pyrolysis chamber. The concentration of CO_2 increases slightly with time. This may be due to the oxidation of the black paint coated on the aluminum foil by oxygen released by AP to a small extent. Since CO_2 is highly absorptive in the IR region, this small increase observed in the transmittance spectra can be neglected for practical purposes. When heated, AP sublimates as well as decomposes. The sublimated AP particles absorb the IR beam resulting in the presence of an AP signal in the transmittance spectra.

The transmittance signal for the regions identified for the products decreases with an increase in time. Hence, the concentrations of the decomposition products of AP increase with time. Mole fractions of the major decomposition products were extracted using the in-house code. Fig. 3(a) shows the variation of mole fractions of the major decomposition products with time. The products' concentration increases with time, reaches a maximum value, and then decreases. The possible explanation for this behaviour is as follows: During pyrolysis of the sample, the product gases evolve and they enter into the IR beam tube from a small hole located at the bottom of the tube just above the sample. The IR beam tube also has a small hole on the diametrically opposite side of the inlet hole as shown in Fig. 1 (c). Hence, there is a constant inflow and outflow of the product gases from the IR beam tube. The IR beam from the FTIR spectrometer passes through the IR beam tube. Hence these evolved products are detected in the IR spectra. As the sample mass reduces, the rate of evolution of the products also decreases. When the sample mass loss is complete, no more products are generated, and hence the gases already present inside the IR beam tube diffuse outwards. The product gases try to equalize the concentration inside the pyrolysis chamber at all locations by mass diffusion. This causes the concentrations of the products to fall from their maximum value.

The products and their concentrations can be found from the recorded IR spectra. Using the same experimental procedure, the process was repeated for set temperatures of 410, 430 and 470°C. The mole fractions reported in the work are average values of at least 3 repetitions at the same set temperature. By changing the set temperature and the rate of evolution of the products, the kinetics parameters for the decomposition of AP were calculated.

The objective of the process of calculation of the kinetic parameters is as follows: (a) Find a global decomposition reaction mechanism (b) Find the kinetic parameters associated with the mechanism found in step a.

A global reaction mechanism for AP can be assumed based on the observed decomposition products:

$$NH_4ClO_4 \xrightarrow{k_j} \text{a}\, H_2O + \text{b}\, HCl + \text{c}\, HNO_3 + \text{d}\ NO_2 + \text{e}\ N_2O + \text{others} \qquad (3)$$

where, k_j - the rate of reaction at jth temperature (s^{-1}, for reaction of first order). a, b, c and d - stoichiometric constants for the products.

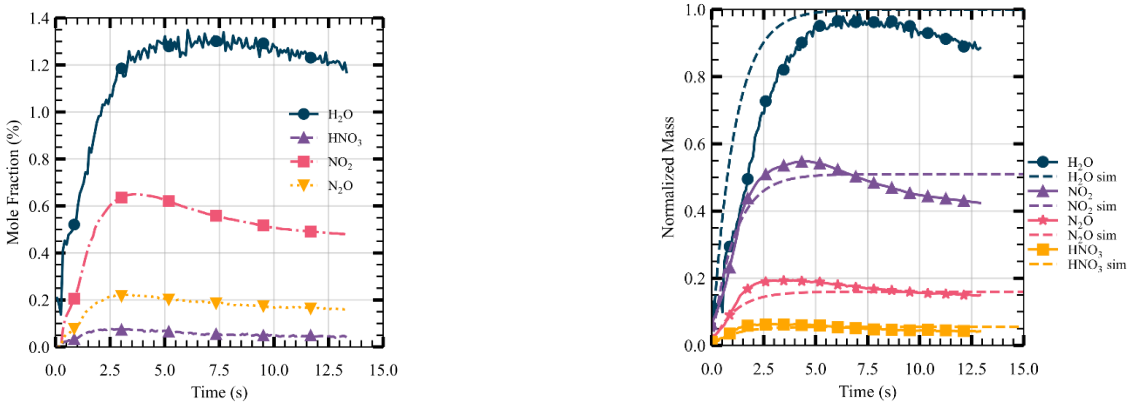

(a) (b)

Fig. 3. (a) Mole fraction profiles of major decomposition products as a function of temperature observed during laser pyrolysis of AP sample at 450 °C (b) Comparison between experimental mole fraction of major decomposition products and mole fraction simulated using the global reaction mechanism and kinetic parameters from laser pyrolyser at 450 ºC.

The rate constant k_j at j^{th} temperature can be expressed in Arrhenius format given by Equation (4) as shown below.

$$K_j(T) = A \times \exp\left(\frac{-E_\alpha}{R_u T_j}\right) \qquad (4)$$

Where, k_j - the rate of reaction at j^{th} temperature (s^{-1} for a first ordered reaction). A - Pre-exponential factor for the rate of reaction (s^{-1} for a first-ordered reaction). E_a - Activation energy of the reaction ($J.mol^{-1}$).R_u - Universal gas constant = 8.314 $J.mol^{-1}.K^{-1}$. T_i - Absolute temperature (K). j - index for temperature. The rate of reaction, stoichiometric coefficient, activation energy and pre-exponential factor are determined by using equation 3 and 4, and FTIR mole fraction data. The ratios of the normalized mole fraction of species were used along with the conservation of atomic masses to formulate the global condensed phase decomposition reaction as given by Equation (5).

$$NH_4ClO_4 \xrightarrow{k_j} 1.09\, H_2O + 0.06\, HNO_3 + 0.56\, NO_2 + 0.18\, N_2O + 0.5\, Cl_2 + 0.71\, O_2 + 0.88 H_2 \qquad (5)$$

Fig. 3(b) represents the comparison between the experimental mole fractions of major decomposition products and the simulated data at 450 ºC. The species profiles have been simulated using a simple one-step global reaction, represented by Equation (5). Similarly, a comparison between the experimental mole fraction of major decomposition products and simulated mole fraction for other set temperatures. The simulated species data demonstrates a reasonable agreement with the experimental data as shown in Fig. 3(b).

The results of kinetics from laser pyrolysis are compared with kinetics obtained from TGA as shown in table 1. Methodology to determine kinetic parameter from TGA is explained in reference [26]. Values obtained from TGA are of of two stages low-temperature decomposition (LTD) and high-temperature decomposition (HTD), whereas, values obtained obtained from rapid pyrolysis give kinetics of a single stage. For comparison, LTD stage kinetics is considered due to its its initial bond-breaking process. The mass loss predicted by the TGA parameters is significantly slower than that predicted predicted by the laser pyrolysis as the rate constant is slow for the TGA experiment as shown in Table 1. Hence, it shows that the TGA parameters are not suitable for simulating pyrolysis under a high heating rate. Thus, for combustion modelling, kinetic parameters obtained from TGA or DSC are not valid at least in the case of AP.

Table 1: Rate constants calculated using kinetic parameters from laser pyrolyser and thermo-gravimetric analysis

Temperature (°C)	The rate constant calculated using E_a *and* A from laser pyrolyser (s^{-1}) (A = 6.6 x 10^7 s^{-1}, E_a = 108 kJ.mol^{-1})	The rate constant calculated using E_a *and* A from TGA (s^{-1}) (A = 5.6 x 10^5 s^{-1}, E_a = 100 kJ.mol^{-1})
410	0.32	0.01
430	0.56	0.02
450	0.93	0.03
470	1.50	0.05

5. Conclusion

A laser pyrolyser setup is developed that can measure the physical quantities necessary to find the kinetics of the condensed phase decomposition under a combustion-like environment. Values of activation energy (E_a) and pre-exponential factor (A) associated with the condensed phase decomposition of AP are 108 kJ.mol^{-1} and 6.6 x 10^7 s^{-1}, respectively, for 50 µm AP at high heating rate and atmospheric pressure. The data obtained from the laser pyrolyser shows clearly that the kinetic parameters obtained from slow heating experiments predict a mass loss rate significantly lower than that observed under high heating rates. This points to the fact that the heating rate plays a significant role in the decomposition mechanism of AP. Determined a single-step global condensed phase decomposition reaction for AP which is representative of the actual complex multi-step chemical reactions.

$$NH_4ClO_4 \xrightarrow{k_j} 1.09\,H_2O + 0.06\,HNO_3 + 0.56\,NO_2 + 0.18\,N_2O + 0.5\,Cl_2 + 0.71\,O_2 + 0.88H_2$$

A robust dataset, consisting of the species profiles at set temperatures and atmospheric pressures, is generated. This data set can be used to develop a detailed multi-step chemical reaction mechanism for the condensed phase decomposition of AP.

Acknowledgements

We extend our gratitude to the High Energy Materials Research Laboratory for providing the AP samples. We are also grateful for the financial support received for this work from DRDO under grant RD/0117-COPTS00-001.

References

[1] M. D. Timken, J. K. Chen, and T. B. Brill, "Thermal Decomposition of Energetic Materials 37. SMATCH/FT-IR (Simultaneous MAss and Temperature CHange/FT-IR) Spectroscopy," Appl Spectrosc, vol. 44, no. 4, pp. 701–706, 1990.

[2] T. B. Brill, P. J. Brush, K. J. James, J. E. Shepherd, and K. J. Pfeiffer, "T-Jump/FT-IR Spectroscopy: A New Entry into the Rapid, Isothermal Pyrolysis Chemistry of Solids and Liquids," Appl Spectrosc, vol. 46, no. 6, pp. 900–911, Jun. 1992.

[3] E. S. Kim, H. S. Lee, C. F. Mallery, and S. T. Thynell, "Thermal decomposition studies of energetic materials using confined rapid thermolysis / FTIR spectroscopy," Combust Flame, vol. 110, no. 1–2, pp. 239–255, Jul. 1997.

[4] N. Kubota, Propellants and Explosives: Thermochemical Aspects of Combustion. Wiley-VCH Verlag GmbH & Co. KGaA, 2015.

[5] M. W. Beckstead, “Recent progress in modeling solid propellant combustion,” Combust Explos Shock Waves, vol. 42, no. 6, pp. 623–641, 2006.
[6] T. L. Jackson, “Modeling of Heterogeneous Propellant Combustion: A Survey,” AIAA Journal, vol. 50, no. 5, pp. 993–1006, May 2012.
[7] C. Dennis and B. Bojko, “On the combustion of heterogeneous AP/HTPB composite propellants: A review,” Fuel, vol. 254, p. 115646, Oct. 2019, doi: 10.1016/J.FUEL.2019.115646.
[8] T. B. Brill, H. Arisawa, P. J. Brush, P. E. Gongwer, and G. K. Williams, “Surface Chemistry of Burning Explosives and Propellants,” J Phys Chem, vol. 99, no. 5, pp. 1384–1392, Feb. 1995.
[9] M. Summerfield, “Burning Mechanism of Ammonium Perchlorate Propellants,” in Solid Propellant Rocket Research, in Progress in Astronautics and Aeronautics. American Institute of Aeronautics and Astronautics, 1960, pp. 141–182.
[10] M. W. Beckstead, R. L. Derr, and C. F. Price, “A model of composite solid-propellant combustion based on multiple flames,” AIAA Journal, vol. 8, no. 12, pp. 2200–2207, Dec. 1970.
[11] A. G. Merzhanov, “The theory of stable homogeneous combustion of condensed substances,” Combust Flame, vol. 13, no. 2, pp. 143–156, Apr. 1969.
[12] G. B. Manelis and V. A. Strunin, “The mechanism of ammonium perchlorate burning,” Combust Flame, vol. 17, no. 1, pp. 69–77, Aug. 1971.
[13] S. C. Li, F. A. Williams, and S. B. Margolis, “Effects of two-phase flow in a model for nitramine deflagration,” Combust Flame, vol. 80, no. 3–4, pp. 329–349, Jun. 1990.
[14] M. W. Beckstead, R. L. Derr, and C. F. Price, “The combustion of solid monopropellants and composite propellants,” Symposium (International) on Combustion, vol. 13, no. 1, pp. 1047–1056, Jan. 1971.
[15] O. P. Korobeinichev, A. S. Shmelev, and A. V Tatevosyan, “Model of the catalysis of burning of a monopropellant (with reference to ammonium perchlorate),” Combust Explos Shock Waves, vol. 8, no. 3, pp. 304–311, 1972.
[16] M. Jeppson, M. Beckstead, and Q. Jing, “A kinetic model for the premixed combustion of a fine AP/HTPB composite propellant,” in 36th AIAA Aerospace Sciences Meeting and Exhibit, in Aerospace Sciences Meetings. American Institute of Aeronautics and Astronautics, 1998.
[17] P. A. Ramakrishna, P. J. Paul, and H. S. Mukunda, “Revisiting the Modeling of Ammonium Perchlorate Combustion: Development of an Unsteady Model,” J Propuls Power, vol. 22, no. 3, pp. 661–668, May 2006.
[18] S. Varunkumar, M. Zaved, and H. S. Mukunda, “A novel approach to composite propellant combustion modeling with a new Heterogeneous Quasi One-dimensional (HeQu1-D) framework,” Combust Flame, vol. 173, pp. 411–424, 2016.
[19] K. Nagendra, C. Vijay, M. Ingole, and P. A. Ramakrishna, “Combustion of Ammonium Perchlorate monopropellant: Role of heat loss,” Combust Flame, vol. 209, pp. 363–375, Nov. 2019.
[20] W. H. Andersen and R. F. Chaiken, “Detonability of Solid Composite Propellants,” ARS Journal, vol. 31, no. 10, pp. 1379–1387, Oct. 1961.
[21] R. L. Coates, “Linear pyrolysis rate measurements of propellant constituents,” AIAA Journal, vol. 3, no. 7, pp. 1257–1261, Jul. 1965.
[22] J. Powling, “Experiments relating to the combustion of ammonium perchlorate-based propellants,” Symposium (International) on Combustion, vol. 11, no. 1, pp. 447–456, 1967.
[23] N. E. Ermolin, O. P. Korobeinichev, A. G. Tereshchenko, and V. M. Fomin, “Kinetic calculations and mechanism definition for reactions in an ammonium perchlorate flame,” Combust Explos Shock Waves, vol. 18, no. 2, pp. 180–189, 1982.
[24] T. B. Brill, P. J. Brush, and D. G. Patil, “Thermal decomposition of energetic materials 60. Major reaction stages of a simulated burning surface of NH4ClO4,” Combust Flame, vol. 94, no. 1, pp. 70–76, 1993.
[25] K. Yogi, S. Krishnan, and S. V. Prabhu, “Separation of conduction and convection heat transfer effects for a metal foamed flat plate impinged by a circular jet,” Int J Heat Mass Transf, vol. 185, p. 122387, Apr. 2022.
[26] S. Saha, A. Chowdhury, N. Kumbhakarna, Errata and comments on “Thermal decomposition of ammonium perchlorate—A TGA–FTIR–MS study: part I” [Thermochim. Acta 610 (2015) 57–68], Thermochim. Acta, vol. 731, 2024, 179639.